X-ray Crystal Structures and Molecular Modelling Studies of Calix[4]dibenzocrowns-6 and Their Alkali Metal Cation Complexes

Véronique Lamare*[a], Jean-François Dozol[a], Franco Ugozzoli[b], Alessandro Casnati[c], and Rocco Ungaro[c]

Commissariat à l'Energie Atomique, Centre de Cadarache, DESD/SEP[a],
F-13108 St. Paul lez Durance Cedex, France
Fax: (internat.) + 33-4-4225-4274 r
E-mail: vero@malabar.cad.cea.f

Dipartimento di Chimica Generale ed Inorganica, Chimica Analitica, Chimica Fisica, Università di Parma,
Centro di Studio per la Strutturistica Diffrattometrica del CNR[b],
Viale delle Scienze, I-43100 Parma, Italy
Fax: (internat.) +39-521-905-557
E-mail: ugoz@ipruniv.cce.unipr.it

Dipartimento di Chimica Organica e Industriale, Università degli Studi di Parma[c],
Viale delle Scienze, I-43100 Parma, Italy
Fax: (internat.) +39-521-905-472
E-mail: casnati@ipruniv.cce.unipr.it and ungaro@ipruniv.cce.unipr.it

Received January 12, 1998

Keywords: X-ray crystal structure / Calix crown / Molecular dynamics / Cesium selectivity / Alkali metal cation complex

We present X-ray structures of complexes of $KClO_4 \cdot H_2O$ and $CsPic \cdot H_2O$ with a new calix[4]arene bearing a dibenzocrown-6 ether bridge. Alkali metal cation complexes with this macrocycle have been studied by molecular dynamics simulations in vacuo, taking account of the counterion, and in an explicit water phase, in order to compare the computed structures to those determined by X-ray crystallography. Two different sets of atomic charges were used in order to evaluate the influence of the electrostatic representation on the computed structures. The results obtained show that MNDO scaled charges give simulation results in better agreement with the available experimental data than MNDO/ESP.

Introduction

Rigid calix[4]arenes incorporating crown ether rings have attracted much interest in recent years due to their versatile selectivity towards alkali cations, which is sensitive to the crown size and to the macrocyclic conformation (cone, partial cone, 1,3-alternate and 1,2-alternate)[1][2][3]. This conformation-dependent selectivity has been studied by molecular dynamics (MD) and free-energy perturbation (FEP) simulations in different explicit solvent phases, and is explained in terms of host/guest complementarity and relative solvation effects[4][5]. Experimental studies carried out on 1,3-alternate calix[4]arene-biscrown-6 derivatives have shown that substitution of one of the oxyethylenic units on the crown by a catechol group greatly improves the extraction of cesium and the Cs^+/Na^+ selectivity from an acidic aqueous phase simulating radioactive liquid waste[6][7]. We have previously performed MD and FEP simulations on these compounds in vacuo and in an explicit water phase[8][9], the results of which were in semi-quantitative agreement with the experimental results of complexation in acetonitrile or methanol[10]. The presence of a catechol unit does not have a significant influence on cesium complexation (although an increase of the structural complementarity is observed by MD in water), but the sodium complexation is disfavoured. Moreover, the increase in cesium extraction from an acidic water phase can be attributed to other phenomena, such as greater extractant lipophilicity, which have not been studied by MD[11]. Thus, the previous method was applied to predict the complexing ability towards alkali metal cations of new calix[4]arene crown-6 ligands in the 1,3-alternate conformation. The first simulations were performed prior to synthesis of the compounds[8][12]. Here, we report on modelling studies of the alkali metal cation complexes with the calix[4]arene dibenzo-crown-6 derivative **1** (Figure 1) and on the X-ray crystal structures of the potassium and cesium complexes. To assess the sensitivity of the simulation results to the force field used in the calculations, two different sets of atomic charges have been used (Figure 2).

Results and Discussion

Structural Features from X-ray Crystallographic Studies

Selected bond lengths and angles for the two complexes are reported in Tables 1a,b,c.

The molecular structures of the two complexes (see Figures 3 and 4) show roughly the same structural architecture. In the two cases, there is a similar stereospatial orientation of the ligand around the cation, with the latter encapsulated in the polar cage created by the oxygen atoms of the dibenzocrown-6 and the two inverted aromatic rings A and C

  1434–193X/98/0808–1559 $ 17.50+.50/0

Figure 1. 1,3-Alternate dioctyloxy calix[4]arene mono(2,4-dibenzo)crown-6 **1**

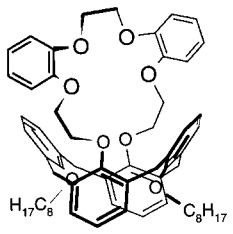

1

Figure 2. Point charges used in simulations

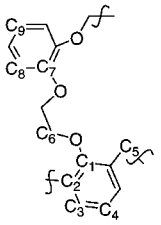

Set 1 MNDO x 1.26		Set 2 MNDO/ESP x 1.42	
C_1 : 0.150	O : -0.346	C_1 : 0.603	O : -0.469
C_2 : -0.119		C_2 : -0.352	
C_3 : -0.020	H_3 : 0.071	C_3 : -0.041	H_3 : 0.133
C_4 : -0.082	H_4 : 0.075	C_4 : -0.239	H_4 : 0.172
C_5 : 0.143	H_5 : 0.001	C_5 : -0.026	H_5 : 0.092
C_6 : 0.220	H_6 : 0.000	C_6 : 0.281	H_6 : 0.000
C_7 : 0.120		C_7 : 0.260	
C_8 : -0.100	H_8 : 0.087	C_8 : -0.231	H_8 : 0.192
C_9 : -0.074	H_9 : 0.080	C_9 : -0.207	H_9 : 0.181
octyl:		octyl:	
C_1 : 0.186	H : 0.00	C : -0.029	H : 0.031
C_2-C_7: -0.002			
C_8 : 0.02			

Table 1a. Selected bond lengths [A] in the **1·KClO$_4$·H$_2$O** and **1·CsPic·H$_2$O** complexes

	1·KClO$_4$·H$_2$O	**1·CsPic·H$_2$O**
$M^{+[a]}$−O1B	3.02(1)	3.068(8)
M^+−O1D	3.08(1)	3.088(6)
M^+−O1*	3.15(1)	3.401(7)
M^+−O2*	3.09(1)	3.335(9)
M^+−O3*	3.14(1)	3.263(12)
M^+−O4*	2.91(1)	3.259(8)
M^+−OW	2.85(1)	
M^+−O1P		3.242(8)
M^+−O7P		3.213(12)
M^+−C3A	3.52(1)	3.64(1)
M^+−C4A	3.34(1)	3.51(1)
M^+−C5A	3.45(2)	3.602(9)
M^+−C3C	3.39(2)	3.75(1)
M^+−C4C	3.27(2)	3.568(1)
M^+−C5C	3.47(2)	3.72(1)

[a] $M^+ = K^+$ or Cs^+.

Table 1b. Selected angles [°] in the **1·KClO$_4$·H$_2$O** complex

O1*−K−OW	57.2(4)	O2*−K−OW	62.1(3)
O2*−K−O1*	47.2(3)	O3*−K−OW	62.5(3)
O3*−K−O1*	94.6(3)	O3*−K−O2*	53.6(3)
O4*−K−OW	93.1(4)	O4*−K−O1*	143.5(3)
O4*−K−O2*	102.4(3)	O4*−K−O3*	50.1(3)
O1D−K−OW	93.0(3)	O1D−K−O1*	53.0(3)
O1D−K−O2*	96.9(3)	O1D−K−O3*	147.4(3)
O1D−K−O4*	160.4(3)	O1B−K−OW	140.6(4)
O1B−K−O1*	160.3(3)	O1B−K−O2*	140.2(3)
O1B−K−O3*	102.3(3)	O1B−K−O4*	55.5(3)
O1B−K−O1D	110.1(3)		

Table 1c. Selected angles [°] in the **1·CsPic·H$_2$O** complex

O1P−Cs−O7P	49.0(3)	O4*−Cs−O7P	107.9(3)
O4*−Cs−O1P	68.1(2)	O3*−Cs−O7P	79.6(3)
O3*−Cs−O1P	71.0(2)	O3*−Cs−O4*	46.1(2)
O2*−Cs−O7P	70.1(3)	O2*−Cs−O1P	101.6(2)
O2*−Cs−O4*	95.8(2)	O2*−Cs−O3*	51.7(2)
O1*−Cs−O7P	78.9(3)	O1*−Cs−O1P	127.4(2)
O1*−Cs−O4*	136.1(2)	O1*−Cs−O3*	95.9(2)
O1*−Cs−O2*	44.4(2)	O1D−Cs−O7P	102.7(3)
O1D−Cs−O1P	136.0(2)	O1D−Cs−O4*	149.4(2)
O1D−Cs−O3*	145.5(2)	O1D−Cs−O2*	96.0(2)
O1D−Cs−O1*	52.0(2)	O1B−Cs−O7P	133.0(3)
O1B−Cs−O1P	85.9(2)	O1B−Cs−O4*	54.0(2)
O1B−Cs−O3*	99.9(2)	O1B−Cs−O2*	143.9(2)
O1B−Cs−O1*	146.4(2)	O1B−Cs−O1D	102.8(2)
C4A−Cs−O7P	135.1(3)	C4A−Cs−O1P	136.9(3)
C4A−Cs−O4*	72.5(3)	C4A−Cs−O3*	69.3(3)
C4A−Cs−O2*	65.3(3)	C4A−Cs−O1*	73.2(3)
C4A−Cs−O1D	87.1(3)	C4A−Cs−O1B	85.0(3)

of the calix[4]arene. However, some significant differences concerning the coordination of the binding sites at the K^+ and Cs^+ cations are apparent.

Figure 3. Perspective view of the **1·KClO$_4$·H$_2$O** complex showing the atom numbering scheme

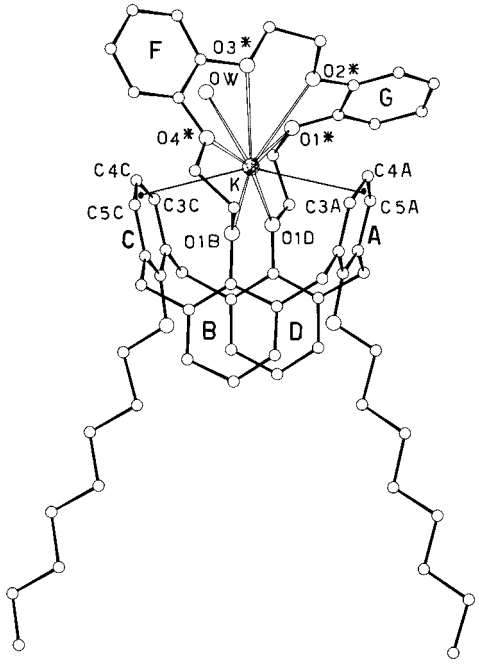

Figure 4. Perspective view of the **1·CsPic·H$_2$O** complex showing the atom numbering scheme

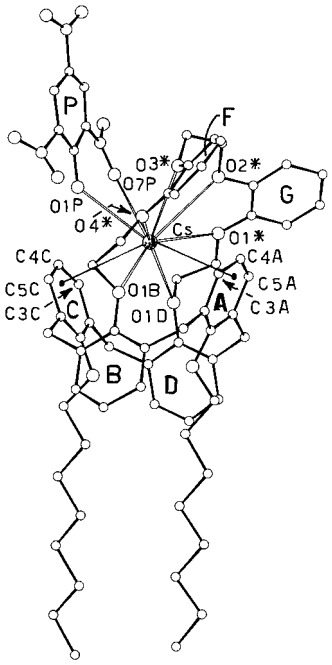

In the **1·CsPic·H$_2$O** complex, the Cs^+ ion (octacoordinated by oxygen atoms) is bound most strongly to the two oxygen atoms of the phenolic units B and D [d(Cs^+−O1B) = 3.068(8) A, d(Cs^+−O1D) = 3.088(6) A]. Moreover, the dibenzocrown-6 moiety is bent to allow the participation of the picrate in the coordination sphere of the cesium ion via its phenoxy oxygen [d(Cs^+−O1P) = 3.242 A] and one oxygen atom of the adjacent NO_2 group [d(Cs^+−O7P) = 3.213(12) A]. The Cs^+−O bond lengths in the coordination sphere are spread over a wide range from 3.068(8) to 3.40(7) A. The water molecule does not interact with the cation but merely fills the voids of the crystal lattice.

In the **1·KClO$_4$·H$_2$O** complex, the K^+−O bond lengths are spread over a narrower range [2.91(3), 3.15(1) A] and the dibenzocrown-6 binds the K^+ ion more symmetrically. The seventh coordination position is occupied by a strongly bound water molecule [d(K^+−OW) = 2.85(1) A], so that the cation is shielded from interactions with the ClO_4^- counterion and the dibenzocrown-6 moiety is less bent than in the Cs^+ complex.

Curiously, comparison of the dihedral angles between the reference plane R (according to ref.[1]) and the least-squares planes of the phenolic rings in the two complexes (Table 2), shows that as the coordination sphere of the cation becomes more regular, the conformation of the 1,3-alternate calixarene moiety becomes less symmetrical. It seems that the strong binding of the two phenolic oxygens O1B and O1D in the Cs^+ complex is responsible of the higher symmetry of the calix[4]arene in the 1,3-alternate conformation, whereas in the K^+ complex the higher symmetry of the coordination sphere is obtained at the expense of symmetry of the calix[4]arene pocket.

Table 2. Dihedral angles [°] between the reference plane R and the least-squares planes though the phenolic rings according to ref.[1]

	1·KClO$_4$·H$_2$O	**1·CsPic·H$_2$O**
A−R	254.7(4)	244.9(2)
B−R	102.1(4)	104.3(8)
C−R	257.3(4)	252.5(3)
D−R	94.8(5)	106.2(3)

Complete descriptions of the calix[4]arene conformations of the two complexes are given by the conformational parameters[13] reported in Table 3, which lead to the C_1 ++, --, ++, -- *symbolic representation* for both calix[4]arenes.

Table 3. Conformational parameters ϕ and κ [°] according to ref.[13]

	1·KClO$_4$·H$_2$O (C_1 ++,−−,++,−−)		**1·CsPic·H$_2$O** (C_1 ++,−−,++,−−)	
	ϕ	κ	ϕ	κ
B−A	123(2)	128(2)	124(1)	132(1)
A−D	−125(2)	−113(2)	−135(1)	−125(1)
D−C	110(2)	127(2)	130(1)	125(1)
C−B	−122(2)	−129(2)	−127(1)	−126(1)

In both complexes, there is structural evidence for a strong cation···π interaction involving the inverted aromatic nuclei A and C. In the K^+ complex, the cation interacts with the aromatic nuclei A and C in an η^3 fashion, via the C3, C4 and C5 atoms, with the shortest distances K^+−C4A [3.34(1) A] and K^+−C4C [3.27(2) A] being significantly shorter than those observed in our previously studied *p-tert*-butylcalix[4]arene diisopropoxy-crown-6 KPic complex in the partial cone conformation[14], and close to the lower limit found by Atwood[15] for a K^+···π interaction.

Also relevant are the two η^3-like cation···π interactions observed in the Cs^+ complex, although the Cs^+···C_ϕ distances to C3, C4 and C5 show that the interactions are stronger for nucleus A rather than for nucleus C. The approach of the latter to the cation is hindered by the presence of the picrate anion.

However, in **1·CsPic·H$_2$O** the Cs^+···C_ϕ distances, which range from 3.51(1) to 3.75(1) A, seem to indicate a weaker cation···π interaction than those observed in our previous studies on diisopropoxycalix[4]arene-crown-6[3] and dimethoxycalix[4]arene-crown-6[16] CsPic complexes, in which the corresponding distances range from 3.486(8) to 3.69(1) A and from 3.354(7) to 3.684(8) A, respectively.

Structural Features from MD Simulations

The atomic charges used in the force field equation (Figure 2) were precalculated on the free ligand using two different semiempirical approaches. With the charges fitted to the molecular electrostatic potential (set 2), the ligand is much more polarized than with the MNDO scaled charges (set 1), which leads to higher electrostatic interactions with the

cation. It was thus of interest to evaluate to what extent the conclusions drawn from MD simulations could be influenced by these parameters.

In the simulations in vacuo, we focused our attention on the structural complementarity between the ligand and the cation, and on the possible perturbations due to a counterion. These simulations were useful in carrying out a rapid screening of the complexing ability of the ligand, and structural data could be compared to available X-ray experimental data, which is our goal in simulations with the calixcrown **1**. The averaged structural data are reported in Table 4, and radial distribution functions around the cation with respect to the six oxygen atoms of the complexed crown, $rdfO_C$, are reported in Table 5. In the $rdfO_C$ curves, the first peak corresponds to the first coordination shell around the cation in the crown environment[17]. The complementarity is regarded as being better, the closer the $rdfO_C$ curve fits the rdf curve corresponding to the distribution of water molecules around the free cation in water[18].

the oxygen atoms. Na^+ is more sensitive to the destabilizing effect of the counterion and is pulled up to the top of the crown, remaining coordinated to four crown oxygen atoms in addition to the bidentate nitrate (Figure 8).

Following these systematic studies, MD simulations were performed in vacuo on the complex with the Cs^+Pic^- ion pair so as to allow closer comparison with the X-ray data. The mean distance values, calculated from a collection of 95 conformations generated during the MD run in vacuo using both sets of charges, show that structural data simulated with charge set 1 fit better to the X-ray geometry than those calculated with set 2 (Table 4 and Figure 9). With set 1, the main difference in the $d(Cs^+-O_C)$ values concerns the phenoxy oxygen atoms (O_P); an almost cylindrical calixarene cavity is generated, with parallel phenyl groups bearing the crown [$d(O_P-O_P)$ = 5.24 (19) A], whereas in the X-ray structure, these are bent so as to give smaller $d(O_P-O_P)$ (4.81 A) and $d(Cs^+-O_P)$ distances. These distances are closer to those of the X-ray structures with set 2, although

Table 4. Average structural data in ligand **1** complexed crown during the MD runs at 300 K

Charges	$d(M^+-$Ocrown)[a]	O1	O2	O3	O4	O5	O6	$<d(M^+-O_C)>$[b]	$<d(M^+-C_4)>$[c]	$d(M^+-$OCR)	$d(M^+-$PlOCR)
ESP × 1.42	**1**·Cs^+	2.94(10)	3.79(29)	3.05(16)	3.45(29)	3.42(25)	3.04(13)	3.28(30)	3.34(4)	1.16(14)	0.09(16)
set 2	Rb^+	2.85(13)	3.86(39)	3.11(27)	3.45(42)	3.34(34)	2.95(17)	3.29(36)	3.20(4)	1.30(20)	0.05(21)
in vacuo	K^+	2.75(12)	3.84(40)	3.13(29)	3.84(51)	3.26(31)	2.95(19)	3.30(42)	3.14(3)	1.37(25)	0.01(19)
	Na^+	2.52(15)	4.20(48)	3.66(43)	4.15(68)	3.19(47)	3.00(34)	3.45(61)	2.95(2)	1.78(30)	0.02(19)
	1·CsPic	3.07(17)	3.64(33)	3.83(32)	3.29(19)	3.32(22)	3.20(17)	3.39(26)	3.38(1)	1.17(19)	0.57(39)
MNDO × 1.26	**1**·Cs^+	3.10(19)	3.34(25)	3.17(21)	3.34(25)	3.26(20)	3.13(18)	3.22(10)	3.41(5)	0.90(18)	0.15(21)
set 1	Rb^+	2.94(14)	3.33(30)	3.08(22)	3.49(36)	3.16(26)	3.00(17)	3.17(19)	3.39(3)	1.01(21)	0.06(23)
in vacuo	K^+	2.86(18)	3.21(39)	3.11(33)	3.33(39)	3.10(34)	2.95(23)	3.09(16)	3.44(3)	1.01(23)	−0.02(19)
	Na^+	2.56(19)	2.79(36)	4.07(59)	3.81(54)	2.84(53)	2.57(22)	3.11(60)	3.36(15)	1.44(33)	0.07(21)
	1·CsPic	3.32(20)	3.24(24)	3.34(25)	3.33(29)	3.28(21)	3.45(29)	3.33(7)	3.59(11)	0.98(18)	0.73(19)
	1·$CsNO_3$	3.30(23)	3.24(22)	3.24(20)	3.62(30)	3.29(20)	3.31(22)	3.33(13)	3.57(2)	1.06(18)	0.76(20)
	$RbNO_3$	3.38(28)	3.17(39)	3.24(37)	3.54(39)	3.16(22)	3.26(30)	3.29(13)	3.54(14)	1.04(23)	0.73(20)
	KNO_3	3.42(34)	3.03(42)	3.13(37)	3.50(47)	3.29(45)	3.39(37)	3.29(17)	3.58(9)	1.06(21)	0.76(24)
	$NaNO_3$	3.44(54)	3.95(97)	2.62(25)	2.61(30)	2.57(39)	4.82(59)	3.33(84)	3.90(11)	1.49(44)	0.77(31)
set 1	**1**·Cs^+ (1729 H_2O)	3.42(31)	3.21(22)	3.41(28)	3.29(29)	3.22(20)	3.40(27)	3.33(9)	3.57(7)	0.97(22)	0.63(32)
in water	Rb^+ (1577 H_2O)	3.46(40)	3.45(39)	3.49(41)	3.14(31)	3.16(26)	3.10(24)	3.29(18)	3.57(1)	1.02(24)	0.70(30)
	K^+ (1439 H_2O)	2.82(15)	3.02(28)	3.06(34)	3.30(40)	3.16(33)	3.37(33)	3.12(18)	3.48(5)	0.78(26)	−0.16(28)
	Na^+ (1389 H_2O)	2.47(13)	2.68(28)	3.97(64)	4.23(60)	2.62(25)	2.52(18)	3.08(73)	3.45(13)	1.52(24)	0.13(47)
	X-ray CsPic	3.07	3.26	3.26	3.34	3.40	3.09	3.24(16)	3.54(2)	0.97	−0.68
	X-ray $K·ClO_4·H_2O$	3.02	2.91	3.14	3.09	3.15	3.08	3.07(16)	3.30(4)	0.67	−0.15

[a] Averages are calculated from 96 snapshots (100 ps), with the exception of **1**·Cs^+ in water (50 snapshots). – [b] Average over the six individual d(M−Oc) values. – [c] Average over two d(M−C*para*) values.

In the absence of a counterion, this peak is quite sharp for the Cs^+ cation, with a rapid return to the baseline, but it broadens as the radius of the cation decreases (Figure 5). The worst complementarity is obtained for Na^+, where the cation is only coordinated to four oxygen atoms with set 1 (Figure 6), or to just three oxygen atoms with set 2 (Figure 7). With the more polarized set of charges 2, all the cations interact mainly with the lower part of the crown, irrespective of the size of the cation (Figure 7).

Simulations were next performed in the presence of the nitrate counterion, using charge set 1. In this case, the cation does not lie in the mean plane of the oxygen atoms of the crown. Cs^+, Rb^+ and K^+ remain coordinated to the six oxygen atoms of the crown, but are shifted towards the upper part of the crown and very far from the barycentre of the cation is unsymmetrically bonded to the crown, and a bad fit with other distances as well as interactions of the cation with the picrate counterion are observed.

The fit of the potassium complex structure was more difficult due to the small cation size, which is more sensitive to the force field conditions, even though the simulation on **1**·K^+ with set 1 achieved the best agreement with the experimental data. To obtain a fit with the X-ray structure, in which a water molecule is coordinated to the potassium cation, simulations were performed in water with charge set 1, starting from a structure minimized after MD in vacuo, and submitted to 100 ps of MD run at 300 K in TIP3P water. This simulation gave a hydrated structure, one water molecule being coordinated to the cation at a facial position [$d(K^+-Ow)$ = 2.7(3) A from the rdfOw curve]. Compared

Table 5. Radial distribution functions around alkali metal cations in water and in the calixcrown during simulations in vacuo

		Na^+	K^+	Rb^+	Cs^+
$d(M^+-O_w)$[a] max [Å]	experiment[40]	2.35(6)	2.79(8)	2.88	3.13(7)
	Aqvist[36]	2.39	2.75	2.89	3.10
	this work[b]	2.5	2.8	2.9	3.2
$rdfO_C$[c]	no. of peaks	2	1	1	1
set 1	$d(M^+-O_C)$ max [Å]	2.5 and 3.4	2.9	3.0	3.1
without nitrate	integral (no. of O_C)	4 and 2	6	6	6
	baseline return [Å]	5.5	4.7	4.4	4.1
$rdfO_C$	no. of peaks	2	1	1	1
set 1	$d(M^+-O_C)$ max [Å]	2.5 and 3.5	3.0	3.2	3.2
with nitrate	integral (no. of O_C)	3.8 and 2.2	6	6	6
	baseline return [Å]	5.8	4.8	4.6	4.5
$rdfO_C$	no. of peaks	2	1	1	1
set 2	$d(M^+-O_C)$ max [Å]	2.7 and 3.5	2.9	2.9	3.0
	integral (no. of O_C)	2.5 and 3.5	6	6	6
	baseline return [Å]	5.5	5.1	4.9	4.7

[a] $d(M^+-O_w)$, distance cation−Owater at the maximum of the first hydration peak.. − [b] rdf curve upon 20 ps of MD run in water. − [c] $rdfO_C$: rdf of the crown′s oxygen atoms around the cation (from 0 to 6 Å) during 100 ps of MD run at 300 K in vacuo.

Figure 5. rdf curves of the O-crown distribution around the cations in the calixcrown during a 100 ps MD run at 300 K in vacuo

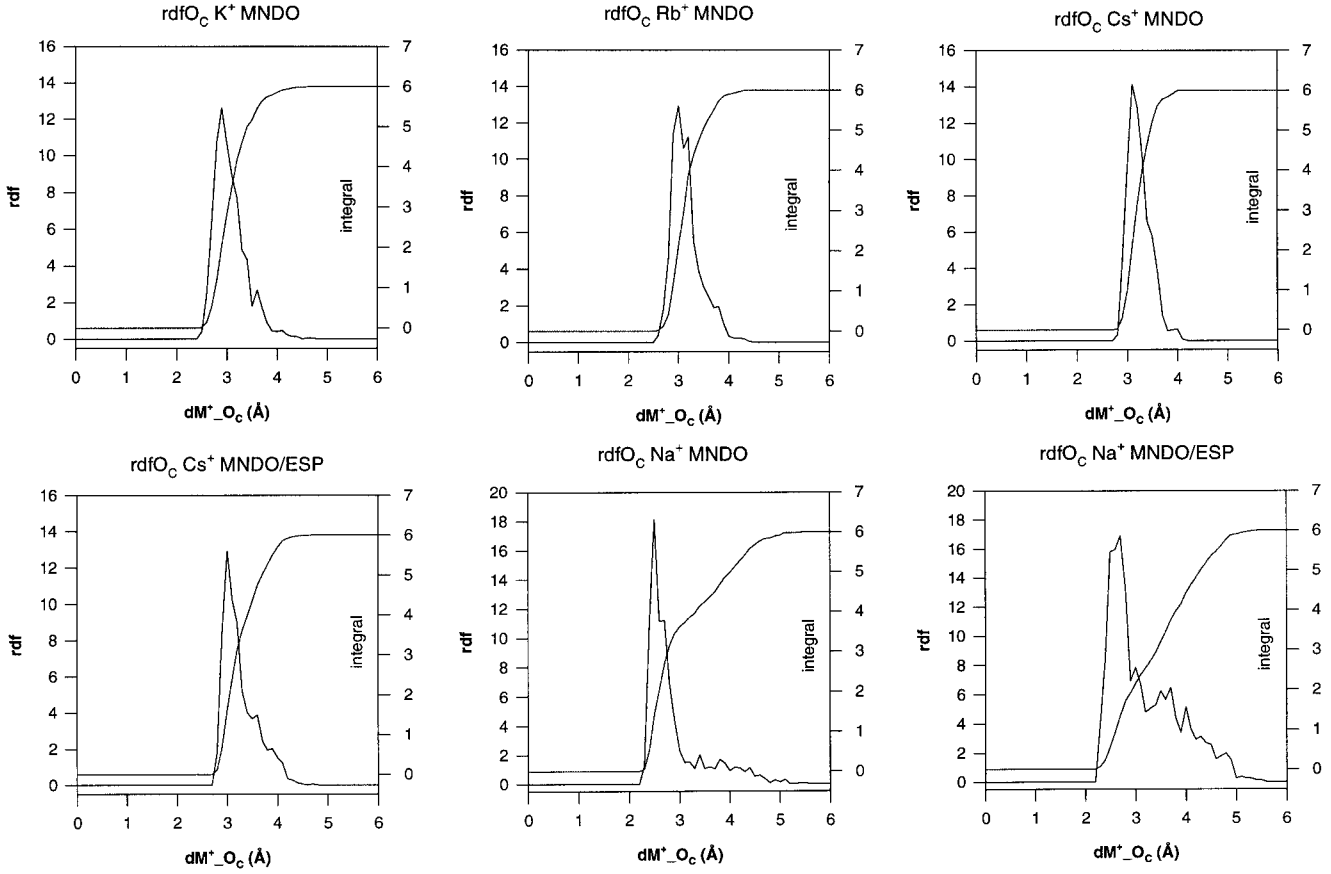

to the X-ray structure, the cation is higher in the crown and interacts more strongly with the coordinated water molecule (Figure 10).

Under the same simulation conditions, the Na^+ cation was not hydrated. This can be justified by the position of the cation near to the barycentre of the crown at the beginning of the simulation in water, which prevents a water molecule from entering the polar niche of the crown. On the other hand, with our former set of charges, which was calculated using the same MNDO scaled method but on half a calixarene, leading to a slightly more polar calixarene cavity, we previously observed on diisopropoxycalix[4]arene-crown-6, that the Na^+ cation was located closer to the phenolic oxygen atoms in the structure minimized in vacuo, allowing one water molecule to enter into the mean plane of the crown above the cation[9]. Since in another study employing the same former set of charges on the 1,3-alternate calix[4]arene-biscrown-6 $(NaNO_3)_2$ complex[19] we found a

Figure 6. Snapshot of alkali metal cation complexes simulated in vacuo with MNDO-scaled charges (100 ps minimized); hydrogen atoms are not represented

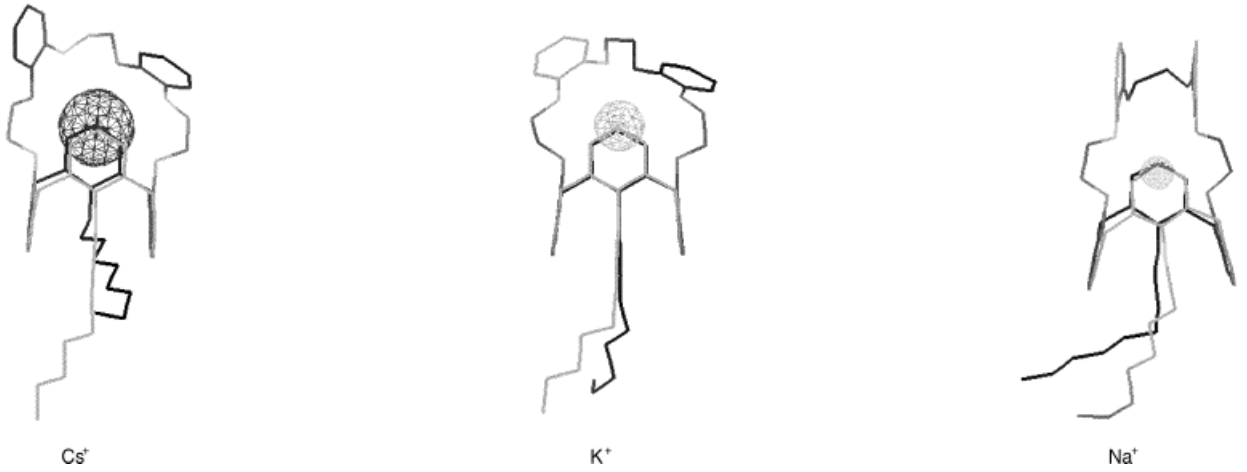

Figure 7. Snapshot of alkali metal cation complexes simulated in vacuo with MNDO/ESP charges (100 ps minimized); hydrogen atoms are not represented

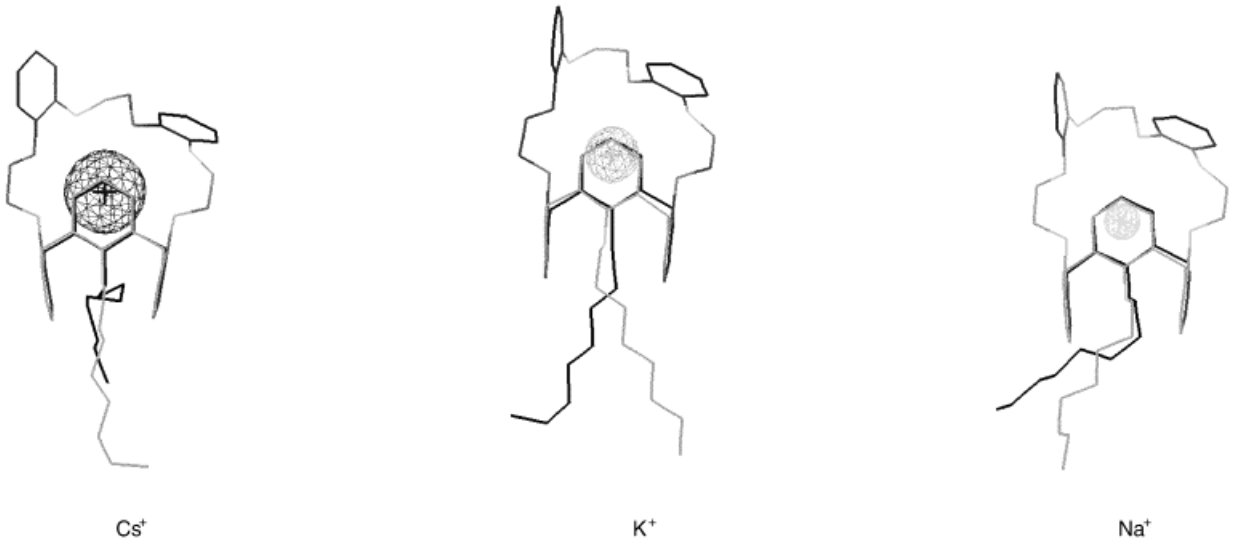

nice agreement between MD calculations and a hydrated X-ray structure, where each Na^+ cation is in interaction with a water molecule located in the lower part of the crown when interactions of the nitrate anions were considered, a computation on the **1**·**Na**$^+$ complex in the presence of the nitrate counterion in water was also performed here. Unfortunately, however, the ion pair underwent decomplexation before hydration.

The simulation of the Cs^+ complex in water with charge set 1 gave structural features close to those of the CsPic complex simulated in vacuo [$<d(Cs^+-Oc)>$ = 3.33(9), $d(Cs^+-OCR)$ = 0.97(22) A]. We observed a water molecule solvating the calixarene cavity, interacting with the two phenoxy oxygen atoms bearing the crown via hydrogen bonds (Figure 10). The cation is well hydrated, as shown by the rdfOw curve, which exhibits one hydration peak around the cation corresponding to 1.5 water molecules. However, decomplexation occurred after 60 ps of MD run in water.

Simulations in water with charge set 2 were performed on Cs^+, K^+, and Na^+ complexes. Cs^+ and K^+ fit the barycentre of the crown more snugly than in vacuo [$<d(Cs^+-Oc)>$ = 3.16(9), $d(Cs^+-OCR)$ = 0.83(14), $<d(K^+-Oc)>$ = 3.22(37), $d(K^+-OCR)$ = 1.18(20) A]. The hydration of the cation is poor, as the rdfOw curve shows only 0.2 water molecules in the first hydration shell of Cs^+, exchanging with bulk water during the whole 100 ps MD run, and no hydration at all for K^+. Like the Cs^+ complex with charge set 1, the three complexes are solvated by one water molecule in the calixarene cavity. This water molecule does not seem to play a significant role in determining the stability of the cationic complexes, except in the case of the Na^+ complex, where it rotated after 70 ps of MD to coordinate the cation, favouring a stronger bonding with the phenolic oxygen atoms bearing the crown.

Selectivity Calculations (Table 6)

Figure 8. Snapshot of alkali metal cation complexes simulated with nitrate counterion in vacuo with MNDO scaled charges (100 ps minimized); hydrogen atoms are not represented

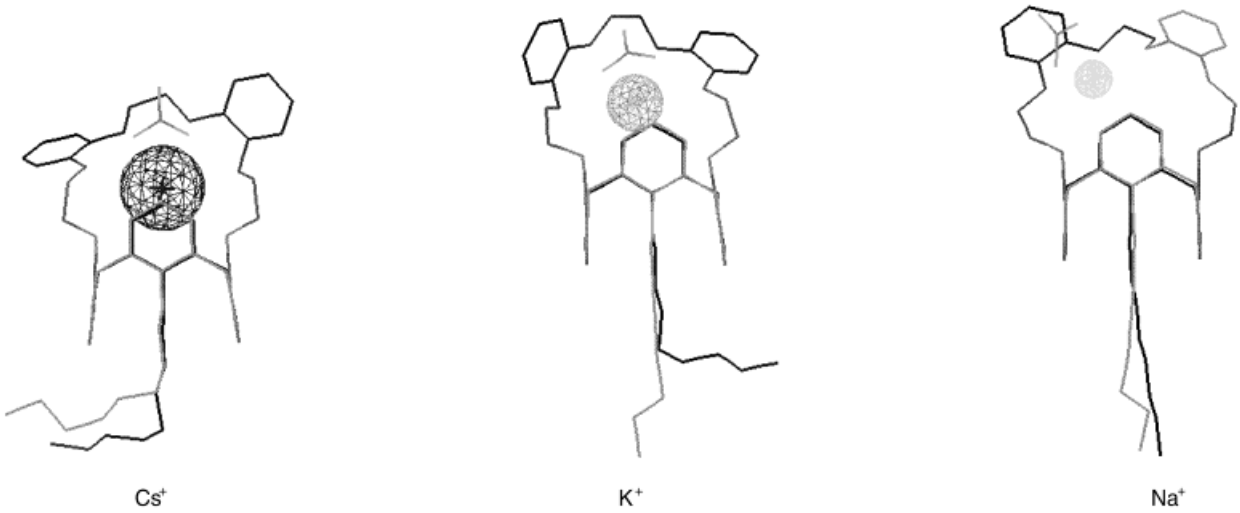

Figure 9. Snapshot of **1**·**CsPic** complexes simulated in vacuo with both sets of charges; hydrogen atoms are not represented

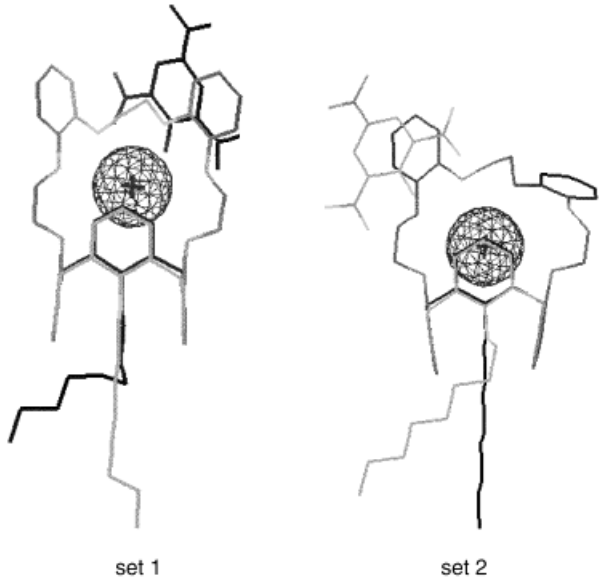

Figure 10. Snapshot of **1**·Cs^+ and **1**·K^+ complexes simulated in water with charge set 1; hydrogen atoms are not represented

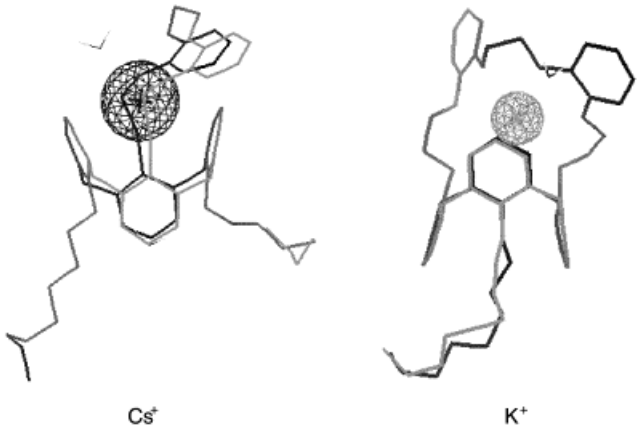

The intrinsic ligand preference towards the cations is calculated by ΔG_{4vac}. The smaller cations are preferred due to the main electrostatic interactions, irrespective of the charge set used. When the relative dehydration energies of the cations ΔG_3 are considered, the differences allow an estimate of the selectivity of extraction for the alkali metal cations into the organic phase, assuming negligible differences in the solvation energies of the cations in the complex, as found in simulations on 1,3-alternate calix[4]arene-biscrown-6 alkali metal cation complexes in chloroform[20][21]. In both cases, the calculations indicate a preference for the bigger cations, although while with charge set 1, the selectivity order is: $Cs^+ > Rb^+ > K^+ >> Na^+$, in accordance with the experimental data (Table 7), with the second set of charges, the calculated selectivity clearly favours Rb^+.

Table 6. ΔG_4 calculated in vacuo from cations mutation on **1**·M^+ complexes without a counterion[a]

charge set	kcal/mol	$Na^+ \rightarrow K^+$	$K^+ \rightarrow Rb^+$	$Rb^+ \rightarrow Cs^+$
	ΔG_3[b]	17.5(0)	5.4(0)	7.8(0)
MNDO × 1.26	ΔG_{4vac}[c]	8.5(2)	3.4(1)	6.9(0)
ESP × 1.42	ΔG_{4vac}[c]	8.3(3)	4.3(0)	8.8(1)

[a] Values are averages of two independent mutations ($M^+ \rightarrow N^+$ and $N^+ \rightarrow M^+$). – [b] TI in a water box 11(2+20) ps (11 windows with 2 ps equilibration and 20 ps data collection). – [c] TI in vacuo 11(2+50) ps or 21(2+50) ps.

Conclusion

On the basis of MD results in vacuo and in an explicit water phase, the best complementarity is found for the Cs^+ cation, which remains almost symmetrically coordinated to the six oxygen atoms of the crown irrespective of the environment around the complex. The complementarity is quite

Table 7. Association constants with **1** for alkali metal picrates in chloroform at 298 K[41]

Cation	K_a (1/M)	ΔG_0
Li^+	1.08×10^5	6.79
Na^+	4.67×10^4	6.30
K^+	6.21×10^7	10.51
Rb^+	8.0×10^8	11.95
Cs^+	1.02×10^9	12.12

satisfactory for Rb^+, although the rdfO_C curve is slightly spread over the optimum value, and one could expect a decrease of selectivity between Cs^+ and Rb^+ compared to the results obtained using the unsubstituted 1,3-alternate calix[4]arene-biscrown-6, due to the larger increase of complementarity towards Rb^+.

Comparison of the molecular geometry obtained from the crystallographic studies with the average structural data obtained from MD simulations in vacuo shows that a fairly good representation of the studied complexes can only be achieved with a classical force field by judicious choice of the charge set. This choice is not straightforward for 1,3-alternate calix[4]arenes, which contain an aromatic cavity interacting with the cation. In the present calculations, as well as in previous ones[4], it has been shown that the best representation is achieved with a slightly polarized charge set on the aromatic part of the calixarene.

The results of selectivity calculations on the new calix crown **1** can be compared to the preliminary experimental data available, e.g. association constants for alkali metal picrates in chloroform (Table 7), which show the selectivity order: $Cs^+ \geq Rb^+ > K^+ >> Li^+ > Na^+$. Thus, our first set of charges gives a better insight into the selectivity than the second one. This is not surprising because MNDO/ESP scaled charges have been shown to reproduce 6-31G*/ESP charges over a large database of molecules[22][23], charges that are recommended for performing calculations in an explicit water phase and to take account of the implicit polarization of two-body water models. These charges are known not to reproduce well the intramolecular interactions[24]. It was not possible to calculate reliable ΔG_{4wat} values in water with set 1, due to decomplexations during long TI/MD runs in water. Like mutations in vacuo, mutations between Cs^+ and Rb^+ in water with set 2 also led to a net selectivity for Rb^+.

From a qualitative point of view, our MD calculations in vacuo and in water with charge set 2 give structural and energetic results in worse agreement with available experimental data than those with set 1, which confirms that the best simulated results are obtained when the modelled calixarene cavity is slightly polarized. Thus, the precalculated set of charges is the key parameter in these force field simulations, and one must be very careful in calculating it. Our current set of charges has so far been reliable in yielding rapid, qualitative information on these calixarene alkali metal cation complexes.

This work was partly supported by the *European Commission* in the framework of the research program "Management and Storage of Radioactive Waste" [grant no. F12-CT90-0062 (TSTS)] and by *COGEMA*.

Experimental Section

Crystal Structure Determination: Single crystals of dimensions ca. 0.2 × 0.3 × 0.4 mm (**1**·**KClO$_4$**·**H$_2$O**) and 0.3 × 0.3 × 0.5 mm (**1**·**CsPic**·**H$_2$O**), suitable for X-ray analyses, were sealed in capillary tubes. The crystal data and the most salient experimental parameters used in the X-ray measurements and in the crystal structure analyses are reported in Table 8. For both compounds, the intensities were calculated from profile analyses according to the Lehmann and Larsen method[25]. During the two data collections, one standard reflection, collected every 100 reflections, showed a linear decay of 10% for **1**·**KClO$_4$**·**H$_2$O** and of 15% for **1**·**CsPic**·**H$_2$O**. The intensities were corrected for Lorentz and polarization effects. Absorption effects were corrected for using ABSORB[26].

The two structures were solved by direct methods using SIR92[27] and then completed by Fourier ΔF map, and were refined by blocked full-matrix least-squares methods on F using SHELX76[28]. In the complex **1**·**KClO$_4$**·**H$_2$O**, one water molecule was found in the coordination sphere of the cation, whereas in the final stages of the refinement of the structure of **1**·**CsPic**·**H$_2$O**, one water molecule, not interacting with the cation, was found in the crystal lattice. − For both complexes, the parameters refined were: the overall scale factor, the atomic coordinates and anisotropic thermal parameters for all non-hydrogen atoms, except for some of the terminal carbon atoms of the aliphatic chains and for the water molecules, which were refined with isotropic thermal parameters.

In the complex **1**·**KClO$_4$**·**H$_2$O**, the ClO_4^- ion was found to be disordered over two different orientations (site occupancy factors of 0.75 and 0.25) with the Cl atom in a common position. The hydrogen atoms were placed at their calculated positions with the geometrical constraint C−H 1.0 A and were refined "riding" on their corresponding carbon atoms. − The atomic scattering factors of the non-hydrogen atoms were taken from Cromer and Waber[29]; the values of $\Delta f'$ and $\Delta f''$ were those of Cromer and Ibers[30]. The geometrical calculations were performed with PARST[31]. All calculations were carried out on the GOULD ENCORE91 of the Centro di Studio per la Strutturistica Diffrattometrica del C.N.R., Parma.

Supplementary Material: For both complexes, tables of anisotropic thermal parameters (tables SI and SIV), tables of the H atoms (tables SII and SV), tables of bond lengths and angles (tables SIII and SVI), and tables of the structure factors are available from F. U. on request. − Crystallographic data (excluding structure factors) for the structure reported in this paper have been deposited with the Cambridge Crystallographic Data Centre as supplementary publication no. CCDC-101591 (Cs) and -101592 (K). Copies of the data can be obtained free of charge on application to CCDC, 12 Union Road, Cambridge CB2 1EZ, UK [Fax: (int. code) + 44(1223)336-033; E-mail: deposit@ccdc.cam.ac.uk; World Wide Web: http://www.ccdc.cam.ac.uk].

Computational Methods: All calculations were carried out on SGI workstations (INDIGO 2 R8000 or Origin 200 R10000) with AMBER 4.1 software[32], using as a force field the all-atom parameters and the following representation of the potential energy[33]:

Table 8. Experimental data of the X-ray diffraction studies

Compound	**1·KClO$_4$·H$_2$O**	**1·CsPic H$_2$O**
Formula	$C_{62}H_{74}O_8 \cdot KClO_4 \cdot H_2O$	$C_{62}H_{74}O_8 \cdot CsC_6H_2N_3O_7 \cdot H_2O$
Crystal system	triclinic	monoclinic
Space group	*P*1bar	$P2_1/c$
Cell parameters at 295K [a]		
a [A]	11.967(2)	14.281(3)
b [A]	25.257(2)	24.695(4)
c [A]	10.162(2)	19.558(3)
α[°]	96.06(2)	90
β [°]	103.61(2)	107.95(2)
γ [°]	80.67(2)	90
V [A^3]	2938.4(9)	6562(2)
Z	2	4
$D_{calcd.}$ [g cm^{-3}]	1.248	1.342
F(000)	1176	2760
molecular mass	1103.83	1326.28
μ [$^{-1}$]	17.16	49.71
diffractometer	Siemens AED	Siemens AED
scan type	θ/2θ	θ/2θ
scan speed [°/min]	3−12	3−12
scan width [°]	[θ − 0.6], [θ + 0.6 + Δλλ^{-1}tg θ]	[θ − 0.6], [θ + 0.6 + Δλλ^{-1}tg θ]
radiation	Cu-K_α (1.54178 A)	Cu-K_α (1.54178 A)
2θ range [°]	6−140	6−140
reflexions measured	±*h*, ±*k*, +*l*	±*h*, +*k*, +*l*
total data measured	11137	13135
criterion for observed	$I \geq 2\sigma(I)$	$I \geq 2\sigma(I)$
unique observed data	3191	3757
No. of variables	229 + 210 + 242	230 + 239 + 185
max. Δ/σ on last cycle	0.08	0.07
$R = \Sigma\|\Delta F\|/\Sigma\|F_o\|$	0.116	0.059
$R_w = \Sigma w^{1/2}\|\Delta F\|/\Sigma w^{1/2}\|F_o\|$	0.116	0.061
GooF = $[\Sigma w^{1/2}\|\Delta F\|^2/(NO - NV)]^{1/2}$	1.946	1.023

[a] Unit cell parameters were obtained by least-squares analysis of the setting angles of 30 (**1·KClO$_4$·H$_2$O**) and 30 (**1·CsPic·H$_2$O**) centered reflections found in a random search of the reciprocal space.

$$E_{pot} = \sum_{bonds} K_r(r - r_{eq})^2 + \sum_{angles} K_\theta(\theta - \theta_{eq})^2 + \sum_{dihedrals} \frac{V_n}{2}(1 + \cos(n\varphi - \eta)) + \sum_{i<j}\left[\varepsilon_{ij}\left(\left(\frac{R^*}{R_{ij}}\right)^{12} - \left(\frac{R^*}{R_{ij}}\right)^{6}\right)\right] + \sum_{i<j}\left[\frac{q_i q_j}{\varepsilon R_{ij}}\right] + \sum_{H\ bonds}\left[\varepsilon_{ij}\left(\left(\frac{R^*}{R_{ij}}\right)^{12} - \left(\frac{R^*}{R_{ij}}\right)^{10}\right)\right]$$

The calixarene model was built on the graphic workstation with InsightII software[34] from previous optimized structures and then submitted to a first minimization with the cesium cation without atomic charges. The atomic charges on the calixarene were calculated using the MNDO semiempirical method without geometry optimization. In the first charge set, they were subsequently averaged for equivalent atoms and scaled up with a 1.26 scaling factor to allow a nice fit with 6-31G*/ESP values commonly used for crown ether moieties[35]. In the second set, they were fitted to the electrostatic molecular potential, scaled up with a 1.42 scaling factor[22], and finally averaged for equivalent atoms. The cation parameters were taken from Aqvist[36] and were adapted to the AMBER force field (TIP3P water model and periodic boundary conditions). The nitrate parameters and the picrate charges were taken from ref.[37] and ref.[20], respectively. The 1−4 non-bonded contributions were scaled down by a factor of 0.5. − In vacuo, the alkali metal cation complexes were submitted to minimization with 50 steepest descent iterations followed by 1950 conjugated gradient iterations. Then, MD simulations were performed at constant temperature (300 K) and energy for 100 ps with a 1.0 fs time step, a dielectric constant set at 1.0, and a 10 A residue-based cut-off. One conformation was saved on each picosecond calculation and the trajectories, built up by the collection of these conformations, were visualized on a graphics screen with MD/DRAW software and analyzed by MDS software[38]. The first five picoseconds, corresponding to the temperature equilibration of the system, were not taken into account in the structural and energetic analysis and averages were calculated over 95 ps of MD. − In water, the MD simulations used a time step of 2.0 fs and a 12 A cut-off. The SHAKE procedure was used to constrain bonds involving hydrogen atoms. We used PBC and an isothermal/isobaric ensemble of 300 K and 1 atm. through coupling to temperature and pressure baths. All the starting structures were complexes minimized at the end of MD runs in vacuo, and were immersed in a TIP3P cubic box, removing water molecules within 2 A of the solute (about 1400−1700 water molecules around the solute). These systems were energy minimized and submitted to at least 100 ps of MD (100 ps of MD in water took approximately 15 CPU hours on the R10000 computer). − Free energy calculations were performed with the thermodynamic integration procedure (TI) and the following thermodynamic cycle was considered[39]:

$$\begin{array}{ccc} calix + M^+ & \xrightarrow{\Delta G_1} & calix : M^+ \\ \downarrow \Delta G_3 & & \downarrow \Delta G_4 \\ calix + N^+ & \xrightarrow{\Delta G_2} & calix : N^+ \end{array}$$

ΔG_3: Relative desolvation energies of the cations (when computed according to the thermodynamic cycle, ΔG_3 is the difference in free energy upon mutating the free cation in the solvent, in this case water). ΔG_4: Difference in free energy upon changing the cation when it is bound to the calixarene in vacuo or in water. The relative binding selectivity is computed by the difference:

$$\Delta\Delta G = \Delta G_1 - \Delta G_2 = \Delta G_3 - \Delta G_4$$

The cation M^+ is mutated into the cation N^+ by dividing the calculation into 11 intermediate states (windows) defined by a coupling factor λ ($\lambda = 1$ initial state, $\lambda = 0$ final state). In vacuo, each window was sampled by 52 ps of MD (2 ps equilibration and 50 ps data collection), summarized in the text by 11(2+50) ps, or by 21(2+50) ps in cases of convergence problems (mutations between Na^+ and K^+). The value reported is the average value between the two mutations $M^+ \rightarrow N^+$ and $N^+ \rightarrow M^+$. The starting point of a mutation was an equilibrated structure at the end of an MD run at 300 K. ΔG_3 was calculated in water for the hydrated cations with TI and the protocol 11(2+20) ps. The cations were previously equilibrated in a 403 TIP3P water box by a 20 ps MD run.

[1] *Calixarenes, A Versatile Class of Macrocyclic Compounds* (Eds.: J. Vicens, V. Böhmer), Kluwer, Dordrecht, **1991**.
[2] A. Arduini, A. Casnati, M. Fabbi, P Minari, A. Pochini, A. R. Sicuri, R. Ungaro, in *Supramolecular Chemistry* (Eds.: V. Balzani, L. De Cola), Kluwer, Dordrecht, **1992**, p. 31−50.
[3] A. Casnati, A. Pochini, R. Ungaro, F. Ugozzoli, F. Arnaud, S. Fanni, M.-J. Schwing, R. J. M. Egberink, F. de Jong, D. N. Reinhoudt, *J. Am. Chem Soc*. **1995**, *117*, 2767−2777.
[4] G. Wipff, M. Lauterbach, *Supramol. Chem.* **1995**, *6*, 187−207.
[5] M. Lauterbach, G. Wipff, in *Phys. Supramol. Chem.*, NATO ASI Series (Eds.: L. Echegoyen, A. Kaifer), Kluwer, Dordrecht, **1996**, p. 1−38.
[6] C. Hill, J.-F. Dozol, V. Lamare, H. Rouquette, S. Eymard, B. Tournois, J. Vicens, Z. Asfari, C. Bressot, R. Ungaro, A. Casnati, *J. Incl. Phenom. Mol. Recog. Chem.* **1994**, *19*, 399−408.
[7] Z. Asfari, C. Bressot, J. Vicens, C. Hill, J.-F. Dozol, H. Rouquette, S. Eymard, V. Lamare, B. Tournois, *Anal. Chem*. **1995**, *67*, 3133−3139.
[8] C. Bressot, *Synthese et modelisation moleculaire de calix[4]arenes fonctionnalises en vue du traitement d'effluents radioactifs*, Ph.D. Thesis, Louis Pasteur University, Strasbourg, France, **1995**.
[9] V. Lamare, C. Bressot, J.-F. Dozol, J. Vicens, Z. Asfari, R. Ungaro, A. Casnati., *Sep. Sci. Technol*. **1997**, *32*, 175−191 (Proc. 9th SST Symp. Gatlinburg, Tennessee, Oct. **1995**).
[10] F. Arnaud-Neu, Z. Asfari, B. Souley, J. Vicens, *New J. Chem*. **1996**, *20*, 453−463.
[11] C. Hill, J.-F. Dozol, H. Rouquette, S. Eymard, B. Tournois. *J. Membr. Sci.* **1996**, *114*, 73−80.
[12] V. Lamare, J.-F. Dozol, Z. Asfari, J. Vicens, F. Arnaud-Neu, S. Fuangfwasdi, P. Thuery, M. Nierlich, Poster P168 presented at 7th ICQC, Atlanta, 9−14 June, **1997** (manuscript in preparation).
[13] F. Ugozzoli, G. D. Andreetti, *J. Incl. Phenom. Mol. Recog. Chem*. **1992**, *13*, 337−348.
[14] F. Ugozzoli, O. Ori, A. Casnati, A. Pochini, R. Ungaro, D. N. Reinhoudt, *Supramol. Chem*. **1995**, *5*, 179−184, and references therein.
[15] J. L. Atwood, *J. Incl. Phenom. Mol. Recog. Chem*. **1985**, *3*, 13−20.
[16] R. Ungaro, A. Casnati, F. Ugozzoli, A. Pochini, J.-F. Dozol, C. Hill, H. Rouquette, *Angew. Chem. Int. Ed. Engl*. **1994**, *33*, 1506−1509.
[17] A. Varnek, C. Sirlin, G. Wipff in *Crystallography of Supramolecular Compounds* (Eds.: G. Tsoucaris et al.), Kluwer Academic Publishers, The Netherlands, **1996**, p. 67−99.
[18] S. Miyamoto, P. A. Kollman, *J. Am. Chem. Soc*. **1992**, *114*, 3668−3674.
[19] P. Thuery, M. Nierlich, V. Lamare, J.-F. Dozol, Z. Asfari, J. Vicens, *Supramol. Chem.* **1997**, *8*, 319−332.
[20] A. Varnek, G. Wipff, *J. Comput. Chem*. **1996**, *17*, 1520−1531.
[21] A. Varnek, G. Wipff, *J. Mol. Struct. (Theochem.)* **1996**, *363*, 67−85.
[22] K. M. Merz Jr., *J. Comput. Chem*. **1992**, *13*, 749−767.
[23] B. H. Besler, K. M. Merz Jr., P.A. Kollman, *J. Comput. Chem*. **1990**, *11*, 432−439.
[24] C. I. Bayly, P. Cieplak, W. D. Cornell, P. A. Kollman, *J. Phys. Chem*. **1993**, *97*, 10269−10280.
[25] M. S. Lehmann, F. K. Larsen, *Acta Crystallogr., Sect. A* **1974**, *30*, 580−584.
[26] F. Ugozzoli, *ABSORB, Comput. Chem*. **1987**, *11*, 109−120.
[27] A. Altomare, M. C. Burla, M. Camalli, G. Cascarano, C. Giacovazzo, A. Guagliardi, G. Polidori, *SIR92, J. Appl. Crystallogr.* **1994**, *27*, 435−436.
[28] G. Sheldrick, *SHELX76, Program for Crystal Structure Determinations*, University of Cambridge, England, **1976**.
[29] D. T. Cromer, J. J. Waber, in *International Tables for X-ray Crystallography* (Eds.: J. A. Ibers, W. C. Hamilton), **1974**, vol. IV, Table 2.2.B, The Kynoch Press, Birmingham, England.
[30] D. T. Cromer, J. A. Ibers, in *International Tables for X-ray Crystallography* (Eds.: J. A. Ibers, W. C Hamilton), **1974**, vol. IV, Table 2.3.1, The Kynoch Press, Birmingham, England.
[31] M. Nardelli, *PARST, Comput. Chem.* **1983**, *7*, 95−98.
[32] D. A. Pearlman, D. A. Case, J. A. Caldwell, W. S. Ross, T. E. Cheatham III, D. M. Ferguson, G. L. Seibel, U. C. Singh, P. Weiner, P. A. Kollman, *AMBER 4.1*, University of California, San Francisco, **1995**.
[33] S. J. Weiner, P. A. Kollman, D. T. Nguyen, D. A. Case, *J. Comput. Chem*. **1986**, *7*, 230−252.
[34] Insight II, Biosym Technologies, San Diego, **1993**.
[35] T. J. Marrone, D. S. Hartsough, K. M. Merz, *J. Phys. Chem.* **1994**, *98*, 1341−1343.
[36] J. Aqvist, *J. Phys. Chem*. **1990**, *94*, 8021−8024.
[37] P. Guilbaud, G. Wipff, *J. Phys. Chem*. **1993**, *97*, 5685−5692.
[38] E. Engler, G. Wipff, *MDS and MD DRAW 2.0.*, Universite Louis Pasteur, Strasbourg, France, **1992**.
[39] P. A. Kollman, *Chem. Rev.* **1993**, *93*, 2395−2417.
[40] Y. Marcus, *Chem. Rev.* **1988**, *88*, 1475−1498.
[41] A. Casnati, R. Ungaro, M. J. Schwing, F. Arnaud, to be published.

[98012]